frontiers | Frontiers in Built Environment

TYPE Original Research
PUBLISHED 23 September 2022
DOI 10.3389/fbuil.2022.971260

OPEN ACCESS

EDITED BY
Massimo Latour,
University of Salerno, Italy

REVIEWED BY
Fabio Freddi,
University College London,
United Kingdom
Antonella Bianca Francavilla,
University of Salerno, Italy

*CORRESPONDENCE
Z. Q. Lang,
z.lang@sheffield.ac.uk

SPECIALTY SECTION
This article was submitted to Earthquake Engineering,
a section of the journal
Frontiers in Built Environment

RECEIVED 16 June 2022
ACCEPTED 09 August 2022
PUBLISHED 23 September 2022

CITATION
Zhu Y-P, Lang ZQ, Fujita K and Takewaki I (2022), The design of nonlinear damped building isolation systems by using mobility analysis. *Front. Built Environ.* 8:971260. doi: 10.3389/fbuil.2022.971260

The design of nonlinear damped building isolation systems by using mobility analysis

Yun-Peng Zhu[1], Z. Q. Lang[1]*, Kohei Fujita[2] and Izuru Takewaki[2]

[1]Department of Automatic Control and Systems Engineering, The University of Sheffield, Sheffield, United Kingdom, [2]Department of Architecture and Architectural Engineering, Kyoto University, Kyoto, Japan

Additional power law nonlinear damping has shown advantages in seismic isolation of buildings. The design of nonlinear damped building isolation systems can be conducted in the frequency domain based on the output frequency response function (OFRF) of the building's frequency output responses. But this often requires many runs of simulations of nonlinear building systems, which will spend a long time when the finite element (FE) model or differential equation model of the building system is complex. In this study, the issue will be resolved by an integrated mobility analysis and equivalent linearization approach. In this approach, the complex linear building system without additional nonlinear damping is represented by several data-driven autoregressive with exogenous input (ARX) models. Mobilities of the building system can be evaluated from these ARX models, so that a mobility-based frequency domain representation of the linear building system can be achieved. After that, an equivalent linearization approach is applied to simulate the building system with additional nonlinear damping. Finally, the OFRF-based design can be conducted based on the proposed mobility analysis and equivalent linearization approach. A 4-degree of freedom (DoF) building system is discussed to demonstrate the advantages of the proposed method. The results indicate that the new approach can significantly increase the efficiency of the design and be effectively applied to the design of complex nonlinear building isolation systems.

KEYWORDS

nonlinear damping, building isolation, mobility, linearization, design

1 Introduction

Power law nonlinear damping has been proven to have many advantages in the vibration control of building structures under earthquake ground motions, that additional power law nonlinear damping can reduce forces and displacements transmitted to buildings over a wide-band frequency range (Lang et al., 2009; Peng et al., 2011). The design of nonlinear damping has been comprehensively studied to achieve a desired building vibration isolation performance (Lang et al., 2013; Menga et al., 2021). For example, Lang et al. (2013) studied the optimal displacement and values of additional nonlinear damping isolators in a multistorey building subject to both harmonic and

earthquake loadings. In general, the design of a nonlinear building isolation system finds optimal nonlinear damping values based on many runs of simulations. The design approach includes the trial-and-error approach and response surface methods (RSMs) (Khuri and Mukhopadhyay, 2010). But this is often ineffective and time-consuming when the finite element (FE) model or differential equations of the building system is complex (Fujita et al., 2014).

For linear systems, complex FE models or differential equations of building systems can be simplified by using mobility analysis (Mak and Jianxin, 2003). Mobility is defined in the frequency domain as the spectrum ratio of velocity and force (Gardonio and Brennan, 2002). Early in 1968, Soliman and Hallam (1968) proposed the mobility power flow approach enabling the analysis of vibration isolations between non-rigid machines and non-rigid foundations. It has shown that, if the mobilities of both non-rigid machines and non-rigid foundations were achieved, the system responses can be calculated in the frequency domain by using these mobilities. Since then, passive solutions using spring and damper to complex linear vibration isolation problems were developed based on the mobility power flow approach for transportation, marine, manufacturing, and construction applications (Koh, 1992; Mak and Su, 2002; Elliott et al., 2004). For example, Mak and Su (2002) applied the mobility analysis to address the occasional occurrence of unsatisfactory performance of vibration isolators observed in isolating vibratory machines placed on a concrete floor. Elliott et al. (2004) discussed the mobility analysis of active vibration isolation systems. Output responses of vibration isolation systems were derived in terms of the mobilities of the two structures connected by an active mount. Then frequency control techniques can be applied to stabilize the vibration isolation system. In practice, most systems are often too complex to theoretically achieve mobilities. In these cases, system mobilities can be directly evaluated from experiments by using modal testing approaches (Cremer and Heckl, 2013). However, this often requires many separate tests on the components of the system (Koh, 1992) to evaluate the mobilities of interest. In this study, system identification is applied to enable the evaluation of building system mobilities using a single experimental test or FE simulation. Autoregressive with exogenous input (ARX) models (Billings, 2013) of the inspected output velocity with respect to the related forces are identified under sufficiently random excitations. Then, the mobilities can be directly evaluated from these ARX models.

Although mobility analysis has been applied to the analysis of many complex vibration isolation systems, it is difficult to extend the idea to study nonlinear damped building isolation systems. The reason behind these difficulties is that the traditional mobility analysis and design is basically a linear approach, which cannot be directly applied to the nonlinear case. The current issue in the design of the building isolation system is the lack of the efficient approach that can be used to simulate nonlinear damped building isolation systems. Recently, Elloit et al. (2015) proved that the output responses of a nonlinear system can be calculated by using an equivalent linear system. In order to resolve the existing issue mentioned earlier, an integrated mobility analysis and equivalent linearization approach will be developed to simulate the building isolation system with additional nonlinear damping.

In practice, the output frequency response functions (OFRFs) have been successfully applied to the frequency design of engineering nonlinear materials and structures (Lang et al., 2007; Zhu and Lang, 2017). The OFRF indicates that nonlinear output spectra subject to demanding loads can be represented by polynomial functions of system design parameters, so that convex optimization and design of system nonlinear dynamics can be conducted (Xiao and Jing, 2015; Zhu and Lang, 2017). In this study, the OFRF representation of the nonlinear damped building isolation system is evaluated based on the numbers of simulations conducted by using the integrated mobility analysis and equivalent linearization approach. After that, an optimization problem is formulated according to the design requirements, and the OFRF representations are implemented to solve the optimal design problem.

The design of a 4- degree of freedom (DoF) nonlinear damped building isolation system will be discussed to demonstrate the application of the proposed analysis and design approach. The results indicate that the design efficiency increases over 50% compared to the traditional design based on solving nonlinear differential equations. The research outcomes are expected to be applied to address seismic isolation problems in various complex building systems.

2 The nonlinear damped building isolation systems

2.1 The model of the building isolation system

Consider a building that can be simplified into a 4-DoF system as illustrated in Figure 1a, where $\ddot{z}(t)$ is the acceleration of the ground motion, the system parameters are defined as

$m_1 = 8.95 \times 10^5$ kg, $m_2 = 8.98 \times 10^5$ kg, $m_3 = 8.70 \times 10^5$ kg,
$m_4 = 5.76 \times 10^5$ kg,
$k_1 = 3.92 \times 10^7$ N/m, $k_2 = 3.09 \times 10^7$ N/m,
$k_3 = 2.67 \times 10^7$ N/m, $k_4 = 1.94 \times 10^7$ N/m,
$c_1 = 6.86 \times 10^5$ Ns/m, $c_2 = 5.41 \times 10^5$ Ns/m,
$c_3 = 4.67 \times 10^5$ Ns/m, $c_4 = 3.4 \times 10^5$ Ns/m.

The linear 4-DoF building system in Figure 1a can be expressed as

$$\mathbf{M}\ddot{\mathbf{x}} + \mathbf{C}\dot{\mathbf{x}} + \mathbf{K}\mathbf{x} = -\mathbf{M}\ddot{\mathbf{z}}(t), \tag{1}$$

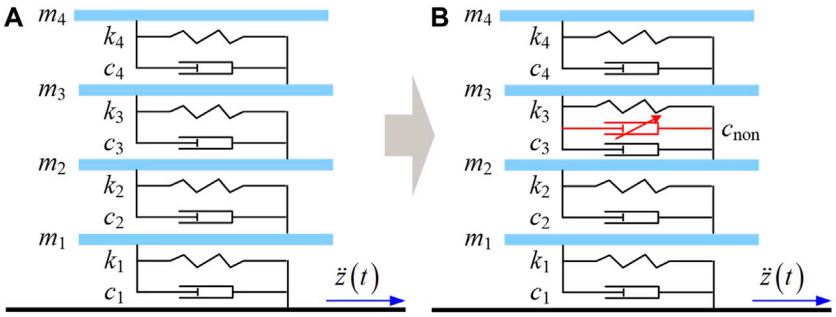

FIGURE 1
4-DoF building system. (A) The linear 4-DoF building, (B) The 4-DoF building with nonlinear damping isolator.

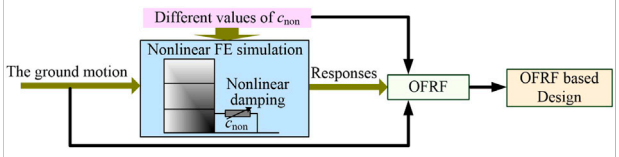

FIGURE 2
Traditional design of nonlinear damped building isolation system.

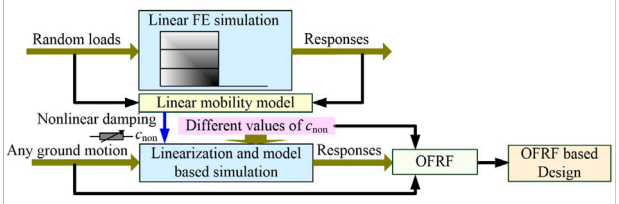

FIGURE 3
New mobility based design of nonlinear damped building isolation system.

where **M**, **C**, and **K** represent mass, damping, and stiffness matrices, respectively.

$$\mathbf{M} = \mathrm{diag}[m_1,\ m_2,\ m_3,\ m_4], \tag{2}$$

$$\mathbf{C} = \begin{bmatrix} c_1 + c_2 & -c_2 & 0 & 0 \\ -c_2 & c_2 + c_3 & -c_3 & 0 \\ 0 & -c_3 & c_3 + c_4 & -c_4 \\ 0 & 0 & -c_4 & c_4 \end{bmatrix}, \tag{3}$$

$$\mathbf{K} = \begin{bmatrix} k_1 + k_2 & -k_2 & 0 & 0 \\ -k_2 & k_2 + k_3 & -k_3 & 0 \\ 0 & -k_3 & k_3 + k_4 & -k_4 \\ 0 & 0 & -k_4 & k_4 \end{bmatrix}. \tag{4}$$

The output vector:

$$\mathbf{x} = [x_1,\ x_2,\ x_3,\ x_4]^{\mathrm{T}}. \tag{5}$$

With x_i for $i = 1, 2, 3, 4$ are the i th floor horizontal displacement relative to the ground, and the absolute horizontal displacement of each floor is given by

$$y_i(t) = x_i(t) + z(t). \tag{6}$$

2.2 The design of nonlinear damped building isolation systems

The aim of the design was to apply an additional nonlinear damping c_{non} to the building system between floors 2 and 3 as shown in Figure 1b, so as to reduce the story drifts between floors 1 and 2, floors 2 and 3, and floors 3 and 4.

In general, the frequency output responses of the nonlinear damped building isolation system can be represented by the OFRF as polynomial functions of the additional nonlinear damping for the system design (Lang et al., 2007). In traditional nonlinear damping design, many runs of simulations of the nonlinear damped building isolation system under different nonlinear damping values are needed to evaluate the OFRF representation. Then the OFRF representation can be applied to implement the system design (Fujita et al., 2014). The design process is illustrated in Figure 2. However, simulations based on solving nonlinear differential equations or applying FE simulations will become inefficient and time-consuming when the building structure is complex.

In order to address this problem, a novel integrated mobility analysis and equivalent linearization of nonlinear damped building isolation system will be developed next. In this approach, only one linear simulation is required to identify a frequency domain representation of building dynamics, known as the linear mobility model, based on which the simulations of the nonlinear damped building isolation system can be conducted much faster than solving the differential equations or applying FE simulations. The new design approach is illustrated in Figure 3 below.

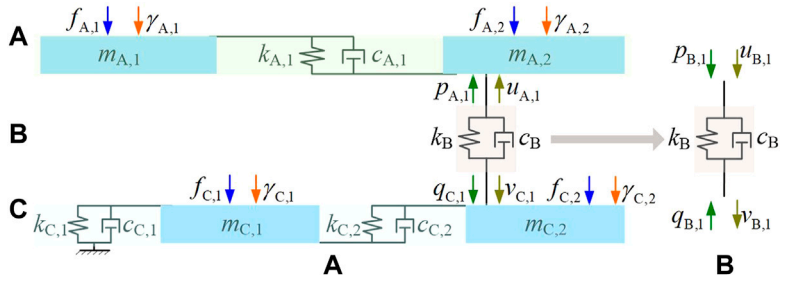

FIGURE 4
Three layer MIMO model of the 4-DoF building isolation system. (A) The three layer MIMO model, (B) The forces and velocities of thee isolator in layer B.

In the following studies, the approach will be developed and demonstrated by using the 4-DoF building isolation system illustrated in Figure 1.

3 The mobility analysis of linear building isolation systems

3.1 The mobility analysis method

The 4-DoF linear building system in Figure 1a can be represented as a 3-layer multiple-input multiple-output (MIMO) vibration isolation system shown in Figure 4a, where

$$\begin{gathered} m_{A,1} = m_4,\ m_{A,2} = m_3,\ m_{C,1} = m_1,\ m_{C,2} = m_2; \\ k_{A,1} = k_4,\ \ k_B = k_3,\ k_{C,1} = k_1,\ k_{C,2} = k_2; \\ c_{A,1} = c_4,\ c_B = c_3,\ c_{C,1} = c_1,\ c_{C,2} = c_2; \\ f_{A,1}(t) = -m_{A,1}\ddot{z}(t);\ f_{A,2}(t) = -m_{A,2}\ddot{z}(t);\ f_{C,1}(t) \\ = -m_{C,1}\ddot{z}(t);\ f_{C,2}(t) = -m_{C,2}\ddot{z}(t); \end{gathered}$$

are input forces induced by the ground motion; $\gamma_{A,1}(t)$, $\gamma_{A,2}(t)$, $\gamma_{C,1}(t)$ and $\gamma_{C,2}(t)$ are input velocities; $q_{C,1}(t)$ and $v_{C,1}(t)$ are the output force and velocity to be evaluated, respectively.

According to the mobility analysis approach (Soliman and Hallam, 1968), the velocity-force relationship of layer A can be represented as

$$\mathbf{U}_A = \mathbf{A}\mathbf{P}_A, \tag{7}$$

where $\mathbf{A}$ is the mobility matrix.

$$\mathbf{U}_A = \begin{bmatrix} \Upsilon_{A,1}(j\omega) \\ \Upsilon_{A,2}(j\omega) \\ U_{A,1}(j\omega) \end{bmatrix};\ \mathbf{A} = \begin{bmatrix} A_{1,1}(j\omega) & A_{1,2}(j\omega) & A_{1,3}(j\omega) \\ A_{2,1}(j\omega) & A_{2,2}(j\omega) & A_{2,3}(j\omega) \\ A_{3,1}(j\omega) & A_{3,2}(j\omega) & A_{3,3}(j\omega) \end{bmatrix};\ \mathbf{P}_A = \begin{bmatrix} F_{A,1}(j\omega) \\ F_{A,2}(j\omega) \\ P_{A,1}(j\omega) \end{bmatrix};$$

where ω is the frequency, $\Upsilon_{A,1}(j\omega)$ and $\Upsilon_{A,2}(j\omega)$ are the spectra of the input velocities $\gamma_{A,1}(t)$ and $\gamma_{A,2}(t)$, respectively; $F_{A,1}(j\omega)$ and $F_{A,2}(j\omega)$ are the spectra of the input forces $f_{A,1}(t)$ and $f_{A,2}(t)$, respectively; $U_{A,1}(j\omega)$ is the spectrum of the output velocity $u_{A,1}(t)$; and $P_{A,1}(j\omega)$ is the spectrum of output force $p_{A,1}(t)$.

The four pole relationship of layer B (Molloy, 1957) can be written as

$$\begin{cases} P_{B,1}(j\omega) = B_{1,1}(j\omega)Q_{B,1}(j\omega) + B_{1,2}(j\omega)V_{B,1}(j\omega), \\ U_{B,1}(j\omega) = B_{2,1}(j\omega)Q_{B,1}(j\omega) + B_{2,2}(j\omega)V_{B,1}(j\omega), \end{cases} \tag{8}$$

where $P_{B,1}(j\omega)$ and $Q_{B,1}(j\omega)$ are the spectra of the forces $p_{B,1}(t)$ and $q_{B,1}(t)$, respectively; $U_{B,1}(j\omega)$ and $V_{B,1}(j\omega)$ are the spectra of the forces $u_{B,1}(t)$ and $v_{B,1}(t)$, respectively; and $B_{i,j}(j\omega)$, $i, j = 1, 2$ are complex numbers defined as (Appendix A).

$$\begin{gathered} B_{1,1}(j\omega) = 1;\ B_{1,2}(j\omega) = 0; \\ B_{2,1}(j\omega) = \frac{j\omega}{k_B + c_B j\omega};\ B_{2,2}(j\omega) = 1. \end{gathered} \tag{9}$$

For layer C, there is

$$\mathbf{V}_C = \mathbf{C}\mathbf{Q}_C, \tag{10}$$

where $\mathbf{C}$ is the mobility matrix.

$$\mathbf{V}_C = \begin{bmatrix} \Upsilon_{C,1}(j\omega) \\ \Upsilon_{C,2}(j\omega) \\ V_{C,1}(j\omega) \end{bmatrix};\ \mathbf{C} = \begin{bmatrix} C_{1,1}(j\omega) & C_{1,2}(j\omega) & C_{1,3}(j\omega) \\ C_{2,1}(j\omega) & C_{2,2}(j\omega) & C_{2,3}(j\omega) \\ C_{3,1}(j\omega) & C_{3,2}(j\omega) & C_{3,3}(j\omega) \end{bmatrix};\ \mathbf{Q}_C = \begin{bmatrix} F_{C,1}(j\omega) \\ F_{C,2}(j\omega) \\ Q_{C,1}(j\omega) \end{bmatrix};$$

where $\Upsilon_{C,1}(j\omega)$ and $\Upsilon_{C,2}(j\omega)$ are the spectra of the input velocities $\gamma_{C,1}(t)$ and $\gamma_{C,2}(t)$, respectively; $F_{C,1}(j\omega)$ and $F_{C,2}(j\omega)$ are the spectra of the input forces $f_{C,1}(t)$ and $f_{C,2}(t)$, respectively; $V_{C,1}(j\omega)$ is the spectrum of the output velocity $v_{C,1}(t)$; and $Q_{C,1}(j\omega)$ is the spectrum of output force $q_{C,1}(t)$.

According to Eqs 7, 10, there are

$$U_{A,1}(j\omega) = A_{3,1}(j\omega)F_{A,1}(j\omega) + A_{3,2}(j\omega)F_{A,2}(j\omega) + A_{3,3}(j\omega)P_{A,1}(j\omega), \tag{11}$$

and

$$V_{C,1}(j\omega) = C_{3,1}(j\omega)F_{C,1}(j\omega) + C_{3,2}(j\omega)F_{C,2}(j\omega) + C_{3,3}(j\omega)Q_{C,1}(j\omega). \tag{12}$$

It is noticed that $P_{A,1}(j\omega) = P_{B,1}(j\omega)$ and $U_{B,1}(j\omega) = -U_{A,1}(j\omega)$, Eq. 11 can be rewritten as

$$-U_{B,1}(j\omega) = A_{3,1}(j\omega)F_{A,1}(j\omega) + A_{3,2}(j\omega)F_{A,2}(j\omega) + A_{3,3}(j\omega)[B_{1,1}(j\omega)Q_{B,1}(j\omega) + B_{1,2}(j\omega)V_{B,1}(j\omega)]. \tag{13}$$

Substituting $Q_{B,1}(j\omega) = Q_{C,1}(j\omega)$ and $V_{B,1}(j\omega) = V_{C,1}(j\omega)$ into Eqs 8, 13, yields

$$\begin{aligned} U_{B,1}(j\omega) &= B_{2,1}(j\omega)Q_{C,1}(j\omega) + B_{2,2}(j\omega)V_{C,1}(j\omega) \\ &= B_{2,2}(j\omega)[C_{3,1}(j\omega)F_{C,1}(j\omega) + C_{3,2}(j\omega)F_{C,2}(j\omega)] \\ &\quad + B_{2,1}(j\omega)Q_{C,1}(j\omega) + B_{2,2}(j\omega)C_{3,3}(j\omega)Q_{C,1}(j\omega), \end{aligned} \tag{14}$$

and

$$\begin{aligned} -U_{B,1}(j\omega) &= A_{3,1}(j\omega)F_{A,1}(j\omega) + A_{3,2}(j\omega)F_{A,2}(j\omega) \\ &\quad + A_{3,3}(j\omega)[B_{1,1}(j\omega)Q_{C,1}(j\omega) + B_{1,2}(j\omega)V_{C,1}(j\omega)] \\ &= A_{3,1}(j\omega)F_{A,1}(j\omega) + A_{3,2}(j\omega)F_{A,2}(j\omega) \\ &\quad + A_{3,3}(j\omega)B_{1,1}(j\omega)Q_{C,1}(j\omega) \\ &\quad + A_{3,3}(j\omega)B_{1,2}(j\omega)[C_{3,1}(j\omega)F_{C,1}(j\omega) + C_{3,2}(j\omega)F_{C,2}(j\omega)] \\ &\quad + A_{3,3}(j\omega)B_{1,2}(j\omega)C_{3,3}(j\omega)Q_{C,1}(j\omega), \end{aligned} \tag{15}$$

respectively.

By adding (14) and (15), the output force $Q_{C,1}(j\omega)$ can be solved as

$$Q_{C,1}(j\omega) = -\frac{1}{M(j\omega)}\begin{Bmatrix} S(j\omega)[C_{3,1}(j\omega)F_{C,1}(j\omega) + C_{3,2}(j\omega)F_{C,2}(j\omega)] \\ + A_{3,1}(j\omega)F_{A,1}(j\omega) + A_{3,2}(j\omega)F_{A,2}(j\omega) \end{Bmatrix}, \tag{16}$$

where

$$\begin{aligned} M(j\omega) &= B_{2,1}(j\omega) + B_{2,2}(j\omega)C_{3,3}(j\omega) + A_{3,3}(j\omega)B_{1,1}(j\omega) \\ &\quad + A_{3,3}(j\omega)B_{1,2}(j\omega)C_{3,3}(j\omega), \\ S(j\omega) &= B_{2,2}(j\omega) + A_{3,3}(j\omega)B_{1,2}(j\omega). \end{aligned}$$

When $Q_{C,1}(j\omega)$ is achieved, the output forces and velocities of each mass can be achieved. For example, $V_{C,1}(j\omega)$ can be calculated from Eq. 10, $U_{B,1}(j\omega) = -U_{A,1}(j\omega)$ can be calculated from Eq. 7.

Therefore, the linear 4-DoF system can be simulated in the frequency domain when the mobilities $A_{1,j}(j\omega)$, $j = 1, 2, 3$, $C_{1,j}(j\omega)$, $j = 1, 2, 3$ are available. Next, the mobility matrices **A** and **C** will be evaluated from several ARX models identified from a single simulation of the linear 4-DoF building system.

3.2 The data-driven–based evaluation of system mobility matrices

Since $V_{C,1}(j\omega) = Y_{C,2}(j\omega)$ and $U_{A,1}(j\omega) = -Y_{A,2}(j\omega)$, the mobility relationships (7) and (10) of layers A and C show that

$$\begin{cases} Y_{A,1}(j\omega) = A_{1,1}(j\omega)F_{A,1}(j\omega) + A_{1,2}(j\omega)F_{A,2}(j\omega) + A_{1,3}(j\omega)P_{A,1}(j\omega), \\ Y_{A,2}(j\omega) = A_{2,1}(j\omega)F_{A,1}(j\omega) + A_{2,2}(j\omega)F_{A,2}(j\omega) + A_{2,3}(j\omega)P_{A,1}(j\omega), \\ A_{3,1}(j\omega) = -A_{2,1}(j\omega);\ A_{3,2}(j\omega) = -A_{2,2}(j\omega);\ A_{3,3}(j\omega) = -A_{2,3}(j\omega), \end{cases} \tag{17}$$

and

$$\begin{cases} Y_{C,1}(j\omega) = C_{1,1}(j\omega)F_{C,1}(j\omega) + C_{1,2}(j\omega)F_{C,2}(j\omega) + C_{1,3}(j\omega)Q_{C,1}(j\omega), \\ Y_{C,2}(j\omega) = C_{2,1}(j\omega)F_{C,1}(j\omega) + C_{2,2}(j\omega)F_{C,2}(j\omega) + C_{2,3}(j\omega)Q_{C,1}(j\omega), \\ C_{3,1}(j\omega) = C_{2,1}(j\omega);\ C_{3,2}(j\omega) = C_{2,2}(j\omega);\ C_{3,3}(j\omega) = C_{2,3}(j\omega). \end{cases} \tag{18}$$

Eqs 17, 18 indicate that the velocities $\gamma_{A,1}(t)$, $\gamma_{A,2}(t)$, $\gamma_{C,1}(t)$, and $\gamma_{C,2}(t)$ can be represented by linear systems with three inputs. In practice, a linear system can be represented in the discrete time domain as an ARX model. For example, $\gamma_{C,2}(t)$ can be represented by the input forces $f_{C,1}(t)$ and $f_{C,2}(t)$, as well as the output force $q_{C,1}(t)$, in discrete time as

$$\begin{aligned} \gamma_{C,2}(k) &= \theta_{\gamma,1}\gamma_{C,2}(k-1) + \cdots + \theta_{\gamma,n_\gamma}\gamma_{C,2}(k-n_\gamma) \\ &\quad + \theta_{f_1,0}f_{C,1}(k) + \cdots + \theta_{f_1,n_{f_1}}f_{C,1}(k-n_{f_1}) \\ &\quad + \theta_{f_2,0}f_{C,2}(k) + \cdots + \theta_{f_2,n_{f_2}}f_{C,2}(k-n_{f_2}) + \theta_{q,0}q_{C,1}(k) \\ &\quad + \cdots + \theta_{q,n_q}q_{C,1}(k-n_q), \end{aligned} \tag{19}$$

where k is the discrete time; n_γ, n_{f_1}, n_{f_2}, and n_q are integers representing the maximum time lags; and $\theta_{\gamma,i}$, $i = 1, \ldots, n_\gamma$; $\theta_{f_1,i}$, $i = 1, \ldots, n_{f_1}$; $\theta_{f_2,i}$, $i = 1, \ldots, n_{f_2}$; and $\theta_{q,i}$, $i = 1, \ldots, n_q$ are model coefficients.

The mobilities of layers A and C can be directly achieved from the ARX model, such as

$$\begin{aligned} C_{3,1}(j\omega) &= \frac{\theta_{f_1,0} + \sum_{k=1}^{n_{f_1}}\theta_{f_1,k}\exp(-jk\omega\Delta t)}{1 - \sum_{k=1}^{n_\gamma}\theta_{\gamma,k}\exp(-jk\omega\Delta t)}, \\ C_{3,2}(j\omega) &= \frac{\theta_{f_2,0} + \sum_{k=1}^{n_{f_2}}\theta_{f_2,k}\exp(-jk\omega\Delta t)}{1 - \sum_{k=1}^{n_\gamma}\theta_{\gamma,k}\exp(-jk\omega\Delta t)}, \\ C_{3,3}(j\omega) &= \frac{\theta_{q,0} + \sum_{k=1}^{n_q}\theta_{q,k}\exp(-jk\omega\Delta t)}{1 - \sum_{k=1}^{n_\gamma}\theta_{\gamma,k}\exp(-jk\omega\Delta t)}, \end{aligned} \tag{20}$$

where Δt is the sampling time applied to the identification of the ARX model.

In order to identify the ARX models, random excitations $f_{A,1}(t)$, $f_{A,2}(t)$, $f_{C,1}(t)$, and $f_{C,2}(t)$ are applied to each floor of

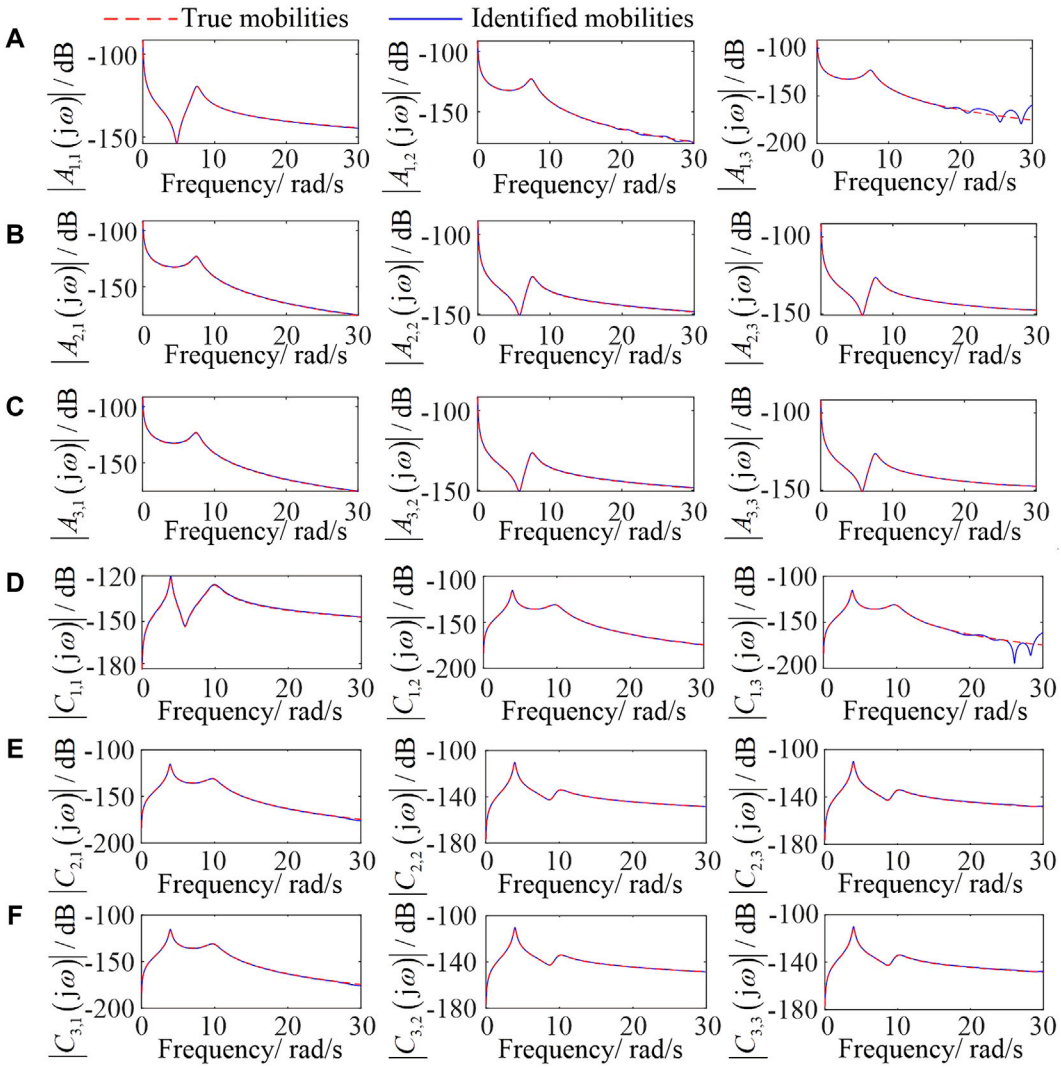

FIGURE 5
Mobilities of the 4-DoF building system. (A-C): The mobilities of layer A, (D-F): The mobilities of layer B.

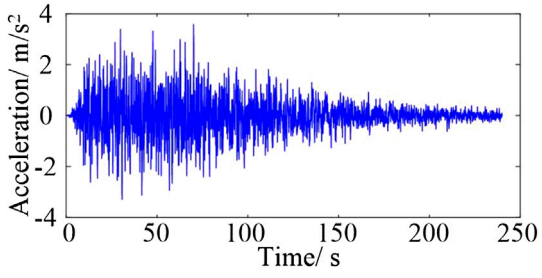

FIGURE 6
Input ground motion.

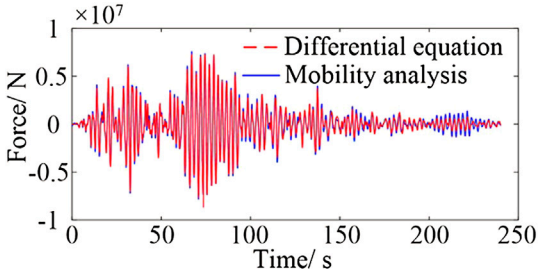

FIGURE 7
Output force of the 4-DoF system.

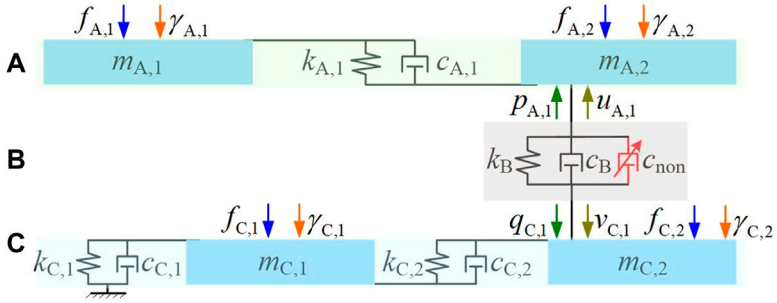

FIGURE 8
Three layer MIMO model of the 4-DoF nonlinear damped building isolation system.

the linear building system. Velocities $\gamma_{A,1}(t)$, $\gamma_{A,2}(t)$, $\gamma_{C,1}(t)$, and $\gamma_{C,2}(t)$, as well as output forces $p_{A,1}(t)$ and $q_{C,1}(t)$ of each floor are collected.

For example, letting $n_\gamma = n_q = n_{f1} = n_{f2} = 70$, the ARX model (19) can be identified. The mobilities $C_{3,1}(j\omega), C_{3,2}(j\omega)$, and $C_{3,3}(j\omega)$ are evaluated by using (20) with $\Delta t = 0.02$ s. The results are shown in Figure 5f, compared with the analytical solutions obtained from the 4-DoF mass-spring-damping system. Other evaluated mobilities are shown in Figures 5a–e.

Subject to a Kokuji wave ground motion shown in Figure 6, the output force spectra $Q_{C,1}(j\omega)$ can be evaluated by using the mobility analysis from (16). The output force $q_{C,1}(t)$ can be achieved as the inverse Fourier transform of $Q_{C,1}(j\omega)$, $\omega \in [0, \pi/\Delta t]$ rad/s as shown in Figure 7. The results were verified by solving the differential Eq. 1 of the linear 4-DoF building system.

4 The analysis and design of nonlinear damped building isolation systems

4.1 The equivalent linearization of nonlinear damped building isolation systems

Consider the 4-DoF building system with additional nonlinear damping in Figure 1b. Denote $w(t) = u_B(t) - v_B(t)$, the additional cubic nonlinear damping force can be represented as

$$f_{non}(t) = c_{non} w(t)^3. \tag{21}$$

The 3-layer representation of the nonlinearly damped 4-DoF system is illustrated in Figure 8.

The nonlinear damped system in Figure 8 can be calculated by the linear mobility approach using equivalent linearization. By finding a linear damping c_{eq} producing equivalent damping force to the nonlinear damping c_{non}, the nonlinear damped system can

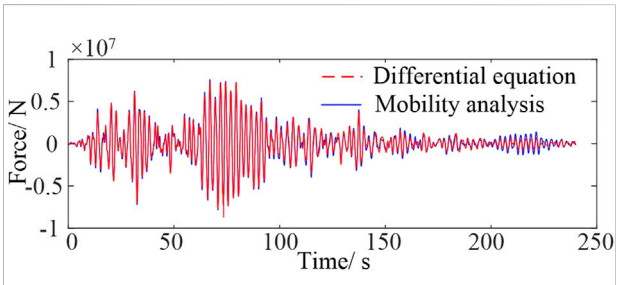

FIGURE 9
Output force of the nonlinearly damped 4-DoF system.

be simulated using the mobility analysis method proposed in Section 3, where the coefficients of the four pole relationship of layer B can be represented as

$$B_{1,1}(j\omega) = 1;\ B_{1,2}(j\omega) = 0;$$
$$B_{2,1}(j\omega) = \frac{j\omega}{k_B + (c_B + c_{eq})j\omega};\ B_{2,2}(j\omega) = 1. \tag{22}$$

Assuming the equivalent damping force is

$$f_{eq}(t) = c_{eq} w(t). \tag{23}$$

The equivalence of the damping force is achieved by the error minimization approach (Elliott et al., 2015). The mean square error (MSE) between the nonlinear damping force and the equivalent linear damping force is

$$MSE = E\left\{\left[f_{non}(t) - f_{eq}(t)\right]^2\right\}, \tag{24}$$

where $E\{.\}$ represents the mean value.

To minimize the MSE (24), letting $\partial MSE/\partial c_{eq} = 0$, yields

$$E\{2\left[f_{non}(t) - c_{eq} w(t)\right] w(t)\} = 0, \tag{25}$$

so that

$$c_{eq} = \frac{E\{f_{non}(t)w(t)\}}{E\{w(t)^2\}} = \frac{E\{c_{non}w(t)^4\}}{E\{w(t)^2\}}. \quad (26)$$

It should be noted that the relative velocity $w(t)$ calculated from the equivalent linear 4-DoF system is also dependent on the equivalent linear damping c_{eq}, the equivalent linear damping c_{eq} can be determined by solving the equation

$$J(c_{eq}) = c_{eq} - \frac{E\{c_{non}w(t)^4\}}{E\{w(t)^2\}} = 0, \quad (27)$$

which can be iteratively solved using a bisection searching algorithm introduced in Appendix B.

Consider the additional nonlinear damping is $c_{non} = 1 \times 10^9$ Ns^3/m^3, the output forces $q_{C,1}(t)$ subject to the ground motion $\ddot{z}(t)$ are shown in Figure 9.

By solving nonlinear differential equations, it took 2.65 s to achieve the output forces, while 1.62 s were needed using the mobility model. The efficiency increases $(2.65 - 1.62)/2.65 = 38.86\%$ in this case. When conducting the design of building isolation systems, many runs of simulations are needed and the new approach will save a lot of time. The efficiency will be further increased as the building system gets complex. For example, when $c_{non} = 1 \times 10^{10}$ Ns^3/m^3, the computing efficiency will increase by 58.44%. This will be discussed in future studies.

4.2 The frequency design of building isolation systems under seismic loadings

The design requirement is to reduce the story drifts $d_{1,2}(t)$, $d_{2,3}(t)$, and $d_{3,4}(t)$ between floors 1 and 2, floors 2 and 3, and floors 3 and 4, respectively. The energy of the story drifts $d_{i,j}(t)$, $(i, j) = (1, 2), (2, 3), (3, 4)$ are defined as

$$E_{i,j} = \int_{t=0}^{\infty} d_{i,j}(t)^2 dt, \ (i, j) = (1, 2), (2, 3), (3, 4). \quad (28)$$

Two optimization problems are discussed as follows.

1) Case study 1

Consider the optimization problem.

Find c_{non} to solve

$$\min_{c_{non}} (E_{1,2} + E_{3,4}).$$

Subject to the constraint

$$c_{non} \in [1, 100] \times 10^7. \quad (29)$$

The output spectrum of the story drifts $D_{i,j}(j\omega)$, $(i, j) = (1, 2), (3, 4)$ can be represented by the OFRF as polynomial functions of nonlinear damping.

$$D_{i,j}(j\omega) = \lambda_0^{(i,j)}(j\omega) + \lambda_1^{(i,j)}(j\omega)c_{non} + \cdots + \lambda_{\bar{N}}^{(i,j)}(j\omega)c_{\bar{N}}^{non}, \quad (30)$$

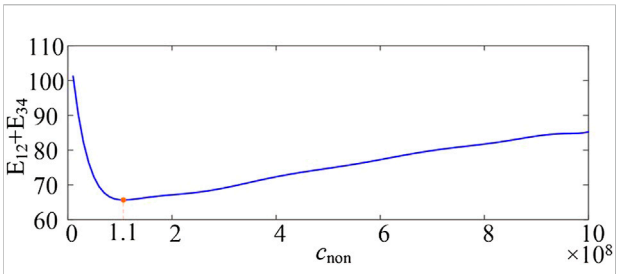

FIGURE 10
Output energy of the nonlinearly damped 4-DoF system. (A) The linear 4-DoF building, (B) The 4-DoF building with nonlinear damping isolator.

where $\lambda_0^{(i,j)}(j\omega)$, $\lambda_1^{(i,j)}(j\omega), \cdots, \lambda_n^{(i,j)}(j\omega)$ are the coefficients, and $\bar{N}$ is the maximum order of the OFRF representation.

Therefore, the energies $E_{i,j}$, $(i, j) = (1, 2), (3, 4)$ can also be represented by the OFRF representation as polynomial functions of the nonlinear damping as

$$E_{i,j} = \varphi_0^{(i,j)} + \varphi_1^{(i,j)}c_{non} + \cdots + \varphi_{\bar{N}}^{(i,j)}c_{\bar{N}}^{non}, \quad (31)$$

where $\varphi_0^{(i,j)}, \varphi_1^{(i,j)}, \cdots, \varphi_{\bar{N}}^{(i,j)}$ are the coefficients.

In order to evaluate the OFRF representations of the energies, the story drift energies are simulated by using the mobility analysis and the equivalent linearization approach under $N \geq \bar{N}$ different values of nonlinear damping. Let $\bar{N} = 10$, $N = 20$ different energy values can be calculated, so that the OFRF representation of energies (31) can be written into matrix forms as

$$\mathbf{E}_{i,j} = \mathbf{C}_{non}\mathbf{\Phi}_{i,j}, \quad (32)$$

where $(i, j) = (1, 2), (3, 4)$.

$$\mathbf{E}_{i,j} = \begin{bmatrix} E_{i,j}^{(1)} \\ \vdots \\ E_{i,j}^{(20)} \end{bmatrix}; \ \mathbf{C}_{non} = \begin{bmatrix} 1 & \cdots & c_{non,(1)}^{10} \\ \vdots & \ddots & \vdots \\ 1 & \cdots & c_{non,(N)}^{10} \end{bmatrix}; \ \mathbf{\Phi}_{i,j} = \begin{bmatrix} \varphi_0^{(i,j)} \\ \vdots \\ \varphi_{10}^{(i,j)} \end{bmatrix}.$$

The coefficients $\mathbf{\Phi}_{i,j}$ can then be evaluated using the least squares (LS) method as

$$\mathbf{C}_{non} = \left(\mathbf{\Phi}_{i,j}^T\mathbf{\Phi}_{i,j}\right)^{-1}\mathbf{\Phi}_{i,j}^T\mathbf{E}_{i,j}. \quad (33)$$

As a result, the OFRF representations of $E_{1,2} + E_{3,4}$ was evaluated as

$$E_{1,2} + E_{3,4} = 116.12 - 17.14 \times 10^{-7}c_{non} + \cdots + 3.98 \times 10^{-85}c_{non}^{10}, \quad (34)$$

and shown in Figure 10.

The optimized nonlinear damping can then be achieved by solving the optimization problems Eqs 28, 29 as $c_{non} = 1.1 \times 10^8$ Ns^3/m^3. The result was validated by solving nonlinear differential equations, showing that by using the new approach, the design efficiency increases by 53.32%.

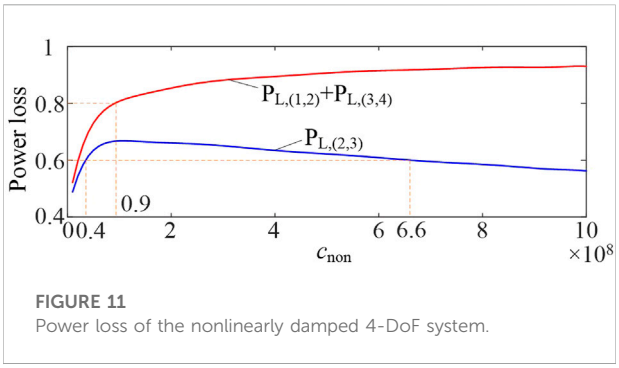

FIGURE 11
Power loss of the nonlinearly damped 4-DoF system.

2) Case study 2

Denote the power loss as

$$P_{L,(i,j)} = 1 - \frac{E_{i,j}}{E_{lin}},\ (i,j) = (1,2),(2,3),\ (3,4), \tag{35}$$

where $E_{i,j}$ are the output energy/power with additional cubic damping, and E_{lin} is the output energy/power of the original linear system.

Consider the optimization problem.

Find

$$\min(c_{non}). \tag{36}$$

Subject to the constraint

$$\begin{cases} c_{non} \in [1,100] \times 10^7, \\ P_{L,(2,3)} \geq 80\%, \\ P_{L,(1,2)} + P_{L,(3,4)} \geq 60\%. \end{cases} \tag{37}$$

According to the discussion in case study 1, the power loss of the nonlinear damped building isolation system can be represented by OFRFs, which were evaluated as

$$\begin{cases} P_{L,(2,3)} = 0.43 + 1.09 \times 10^{-8} c_{non} + \cdots - 1.48 \times 10^{-87} c_{non}^{10}, \\ P_{L,(1,2)} + P_{L,(3,4)} = 0.42 + 8.4 \times 10^{-9} c_{non} + \cdots - 1.31 \times 10^{-87} c_{non}^{10}, \end{cases} \tag{38}$$

and shown in Figure 11.

The optimized nonlinear damping can then be achieved as $c_{non} = 0.9 \times 10^8$ Ns^3/m^3. The result was validated by solving nonlinear differential equations, showing that by using the new approach, the design efficiency increases by 50.51%.

5 Conclusion

The design of a nonlinear damped building isolation system based on many runs of FE simulations or differential equations is often inefficient and time-consuming. For linear vibration isolation systems, mobility analysis can produce more efficient simulation processes than FE or differential equation methods. However, traditional mobility analysis requires separate tests or simulations on system components, and can only be applied to study linear systems. In order to solve these issues in the design of nonlinear damped building isolation systems, a novel data-driven–based evaluation of mobilities and equivalent linearization of nonlinear damping were developed in this study. For a linear building system, several ARX models can be identified from a single test of the building system to evaluate system mobilities. After that, the building system with additional nonlinear damping was simulated by using the equivalent linearization approach, based on which the OFRF-based design of nonlinear damping was conducted. Two case studies on the design of a 4-DoF nonlinear damped building isolation system were discussed. The results indicate the design efficiency increases by over 50% compared to traditional design methods.

In summary, the new approach is more efficient than traditional methods because the mobility model of a complex building isolation system is much simpler than a differential equation or FE model. Such a model can be achieved through a single test on the differential equation or FE model. After that, all the designs can be conducted based on the mobility model. The proposed approach can be extended to more complex building systems to further increase the design efficiency. Moreover, the results can also be applied to nonlinear vibration isolation design in manufacturing and vehicle engineering.

Data availability statement

The original contributions presented in the study are included in the article/Supplementary Material; further inquiries can be directed to the corresponding author.

Author contributions

Y-PZ and ZQL developed the method applied in this manuscript; KF and IT provide the case study and necessary support from the engineering aspect to complete the manuscript.

Funding

This work was supported by the United Kingdom EPSRC grant: EP/R032793/1.

Conflict of interest

The authors declare that the research was conducted in the absence of any commercial or financial relationships that could be construed as a potential conflict of interest.

Publisher's note

References

Billings, S. A. (2013). *Nonlinear system identification: NARMAX methods in the time, frequency, and spatio-temporal domains*. New Jersey, United States: John Wiley & Sons.

Cremer, L., and Heckl, M. (2013). *Structure-borne sound: Structural vibrations and sound radiation at audio frequencies*. Berlin, Germany: Springer Science & Business Media.

Elliott, S. J., Benassi, L., Brennan, M. J., Gardonio, P., and Huang, X. (2004). Mobility analysis of active isolation systems. *J. Sound Vib.* 271 (1-2), 297–321. doi:10.1016/s0022-460x(03)00770-3

Elliott, S. J., Tehrani, M. G., and Langley, R. S. (2015). Nonlinear damping and quasi-linear modelling. *Phil. Trans. R. Soc. A* 373, 20140402. doi:10.1098/rsta.2014.0402

Fujita, K., Kasagi, M., Lang, Z. Q., Guo, P. F., and Takewaki, I. (2014). Optimal placement and design of nonlinear dampers for building structures in the frequency domain. *Earthquakes Struct.* 7 (6), 1025–1044. doi:10.12989/eas.2014.7.6.1025

Gardonio, P., and Brennan, M. J. (2002). On the origins and development of mobility and impedance methods in structural dynamics. *J. Sound Vib.* 249 (3), 557–573. doi:10.1006/jsvi.2001.3879

Khuri, A. I., and Mukhopadhyay, S. (2010). Response surface methodology. *WIREs. Comp. Stat.* 2 (2), 128–149. doi:10.1002/wics.73

Koh, Y. K. (1992). "Prediction and control of vibrational power transmission between coupled structural systems," (United Kingdom: University of Southampton). Doctoral dissertation.

Lang, Z. Q., Billings, S. A., Yue, R., and Li, J. (2007). Output frequency response function of nonlinear Volterra systems. *Automatica* 43 (5), 805–816. doi:10.1016/j.automatica.2006.11.013

Lang, Z. Q., Guo, P. F., and Takewaki, I. (2013). Output frequency response function based design of additional nonlinear viscous dampers for vibration control of multi-degree-of-freedom systems. *J. Sound Vib.* 332 (19), 4461–4481. doi:10.1016/j.jsv.2013.04.001

Lang, Z. Q., Jing, X. J., Billings, S. A., Tomlinson, G. R., and Peng, Z. K. (2009). Theoretical study of the effects of nonlinear viscous damping on vibration isolation of sdof systems. *J. Sound Vib.* 323 (1-2), 352–365. doi:10.1016/j.jsv.2009.01.001

Mak, C. M., and Jianxin, S. (2003). A study of the effect of floor mobility on structure-borne sound power transmission. *Build. Environ.* 38 (3), 443–455. doi:10.1016/s0360-1323(02)00185-3

Mak, C. M., and Su, J. X. (2002). A power transmissibility method for assessing the performance of vibration isolation of building services equipment. *Appl. Acoust.* 63 (12), 1281–1299. doi:10.1016/s0003-682x(02)00047-6

Menga, N., Bottiglione, F., and Carbone, G. (2021). Nonlinear viscoelastic isolation for seismic vibration mitigation. *Mech. Syst. Signal Process.* 157, 107626. doi:10.1016/j.ymssp.2021.107626

Molloy, C. T. (1957). Use of four-Pole parameters in vibration calculations. *J. Acoust. Soc. Am.* 29 (7), 181–853. doi:10.1121/1.1918522

Peng, Z. K., Lang, Z. Q., Zhao, L., Billings, S. A., Tomlinson, G. R., and Guo, P. F. (2011). The force transmissibility of MDOF structures with a non-linear viscous damping device. *Int. J. Non-Linear Mech.* 46 (10), 1305–1314. doi:10.1016/j.ijnonlinmec.2011.06.009

Soliman, J. I., and Hallam, M. G. (1968). Vibration isolation between non-rigid machines and non-rigid foundations. *J. Sound Vib.* 8 (2), 329–351. doi:10.1016/0022-460x(68)90236-8

Xiao, Z., and Jing, X. (2015). Frequency-domain analysis and design of linear feedback of nonlinear systems and applications in vehicle suspensions. *Ieee. ASME. Trans. Mechatron.* 21 (1), 1–517. doi:10.1109/tmech.2015.2446519

Zhu, Y., and Lang, Z. Q. (2017). Design of nonlinear systems in the frequency domain: An output frequency response function-based approach. *IEEE Trans. Control Syst. Technol.* 26 (4), 1358–1371. doi:10.1109/tcst.2017.2716379

Appendix A

In layer B, the forces and velocities on the linear isolator are shown in Figure A1.

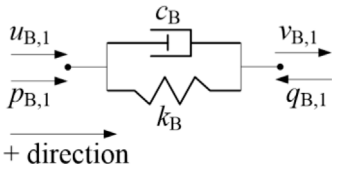

FIGURE A1
Forces and velocities of the isolator.

In Figure A1, there are

$$p_{B,1}(t) = q_{B,1}(t) = k_B\left[\int u_{B,1}(t)\mathrm{d}t - \int v_{B,1}(t)\mathrm{d}t\right] + c_B\left[u_{B,1}(t) - v_{B,1}(t)\right]. \tag{A1}$$

In the frequency domain, (A1) can be rewritten as

$$\begin{cases} P_{B,1}(j\omega) = \dfrac{k_B}{j\omega}\left[U_{B,1}(j\omega) - V_{B,1}(j\omega)\right] + c_B\left[U_{B,1}(j\omega) - V_{B,1}(j\omega)\right], \\ P_{B,1}(j\omega) = Q_{B,1}(j\omega). \end{cases} \tag{A2}$$

It is noticed that

$$\begin{cases} P_{B,1}(j\omega) = B_{1,1}(j\omega)Q_{B,1}(j\omega) + B_{1,2}(j\omega)V_{B,1}(j\omega), \\ U_{B,1}(j\omega) = B_{2,1}(j\omega)Q_{B,1}(j\omega) + B_{2,2}(j\omega)V_{B,1}(j\omega). \end{cases} \tag{A3}$$

$B_{i,j}(j\omega)$, $i, j = 1, 2$ can be evaluated as (9).

Appendix B

Algorithm 1. The bisection searching algorithm

Step 1:	**Initialize:** A random selection of $c_{eq} \in \left(0, c_{eq,max}\right)$; A positive threshold $\rho \ll 1$;
Step 2:	**Random bisection approach:** $c_0^- = 0, c_0^+ = c_{eq,max}$; *while* $\left\|J\left(c_{eq}\right)\right\| / c_{eq} > \rho$ Randomly select $c_{eq} \in \left[c_0^-, c_0^+\right]$; If $J\left(c_{eq}\right) < 0 \rightarrow c_0^- = c_{eq}$; If $J\left(c_{eq}\right) > 0 \rightarrow c_0^+ = c_{eq}$; *end*
Step 3:	**Output:** Equivalent linear damping c_{eq}.